References and Notes

1. M. Born, E. Wolf, Eds., *Principle of Optics* (Cambridge Univ. Press, Cambridge, 1998).
2. J. B. Pawley, Ed., *Handbook of Biological Confocal Microscopy* (Springer, New York, ed. 3, 2006).
3. E. Abbe, *Arch. Mikrosk. Anat.* **9**, 413 (1873).
4. M. G. Gustafsson *et al.*, *Biophys. J.*, in press; published online 7 March 2008 (10.1529/biophysj.107.120345).
5. M. G. Gustafsson, *J. Microsc.* **198**, 82 (2000).
6. R. Heintzmann, G. Ficz, *Brief. Funct. Genomics Proteomics* **5**, 289 (2006).
7. S. W. Hell, *Nat. Biotechnol.* **21**, 1347 (2003).
8. S. W. Hell, *Science* **316**, 1153 (2007).
9. R. J. Kittel *et al.*, *Science* **312**, 1051 (2006); published online 13 April 2006 (10.1126/science.1126308).
10. K. I. Willig, S. O. Rizzoli, V. Westphal, R. Jahn, S. W. Hell, *Nature* **440**, 935 (2006).
11. Material and methods are available on *Science* Online.
12. R. Reichelt *et al.*, *J. Cell Biol.* **110**, 883 (1990).
13. B. Burke, C. L. Stewart, *Nat. Rev. Mol. Cell Biol.* **3**, 575 (2002).
14. M. R. Paddy, A. S. Belmont, H. Saumweber, D. A. Agard, J. W. Sedat, *Cell* **62**, 89 (1990).
15. M. Beck *et al.*, *Science* **306**, 1387 (2004); published online 28 October 2004 (10.1126/science.1104808).
16. M. Beck, V. Lucic, F. Forster, W. Baumeister, O. Medalia, *Nature* **449**, 611 (2007).
17. D. Stoffler *et al.*, *J. Mol. Biol.* **328**, 119 (2003).
18. D. A. Agard, Y. Hiraoka, P. Shaw, J. W. Sedat, *Methods Cell Biol.* **30**, 353 (1989).
19. H. Albiez *et al.*, *Chromosome Res.* **14**, 707 (2006).
20. L. Gerace, A. Blum, G. Blobel, *J. Cell Biol.* **79**, 546 (1978).
21. B. Fahrenkrog *et al.*, *J. Struct. Biol.* **140**, 254 (2002).
22. R. Tonini, F. Grohovaz, C. A. Laporta, M. Mazzanti, *FASEB J.* **13**, 1395 (1999).
23. M. Winey, D. Yarar, T. H. Giddings Jr., D. N. Mastronarde, *Mol. Biol. Cell* **8**, 2119 (1997).
24. M. Fricker, M. Hollinshead, N. White, D. Vaux, *J. Cell Biol.* **136**, 531 (1997).
25. M. Bates, B. Huang, G. T. Dempsey, X. Zhuang, *Science* **317**, 1749 (2007); published online 15 August 2007 (10.1126/science.1146598).
26. E. Betzig *et al.*, *Science* **313**, 1642 (2006); published online 9 August 2006 (10.1126/science.1127344).
27. G. Donnert *et al.*, *Proc. Natl. Acad. Sci. U.S.A.* **103**, 11440 (2006).
28. B. Huang, W. Wang, M. Bates, X. Zhuang, *Science* **319**, 810 (2008); published online 2 January 2008 (10.1126/science.1153529).
29. M. J. Rust, M. Bates, X. Zhuang, *Nat. Methods* **3**, 793 (2006).

30. This work was supported by grants from the Bavaria California Technology Center, the Center for NanoScience, the Nanosystems Initiative Munich, and the Deutsche Forschungsgemeinschaft to L. Schermelleh, M.C.C., and H.L.; by NIH grant GM-2501–25 to J.W.S.; by the David and Lucile Packard Foundation; and by NSF through the Center for Biophotonics, an NSF Science and Technology Center managed by the University of California, Davis, under cooperative agreement no. PHY 0120999. P.M.C. is partially supported by the Keck Laboratory for Advanced Microscopy at the University of California, San Francisco. We thank A. Čopič, K. Weis, and F. Spada for comments on the manuscript and helpful discussions. P.M.C., L. Shao, L.W., and P.K. have performed limited paid consulting for Applied Precision, which is planning a commercial microscope system using three-dimensional structured illumination. The University of California holds patents for structured illumination microscopy.

Supporting Online Material

www.sciencemag.org/cgi/content/full/320/5881/1332/DC1
Materials and Methods
Figs. S1 to S6
References and Notes
Movies S1 and S2

25 February 2008; accepted 13 May 2008
10.1126/science.1156947

Intersection of the RNA Interference and X-Inactivation Pathways

Yuya Ogawa, Bryan K. Sun, Jeannie T. Lee*

In mammals, dosage compensation is achieved by X-chromosome inactivation (XCI) in the female. The noncoding *Xist* gene initiates silencing of the X chromosome, whereas its antisense partner *Tsix* blocks silencing. The complementarity of Xist and Tsix RNAs has long suggested a role for RNA interference (RNAi). Here, we report that murine Xist and Tsix form duplexes in vivo. During XCI, the duplexes are processed to small RNAs (sRNAs), most likely on the active X (Xa) in a Dicer-dependent manner. Deleting *Dicer* compromises sRNA production and derepresses *Xist.* Furthermore, without Dicer, Xist RNA cannot accumulate and histone 3 lysine 27 trimethylation is blocked on the inactive X (Xi). The defects are partially rescued by truncating Tsix. Thus, XCI and RNAi intersect, down-regulating *Xist* on Xa and spreading silencing on Xi.

X-chromosome inactivation (XCI) (*1*) balances X-chromosome dosages between XX and XY individuals. XCI is initiated by *Xist* (*2*, *3*) and opposed by *Tsix* (*4*). How *Xist* induces XCI on inactive X (Xi) and how *Tsix* stably silences *Xist* on active X (Xa) remain two unanswered questions. A role for RNA interference (RNAi) has long been speculated. RNAi refers to the repressive influence of double-stranded RNA (dsRNA) on gene transcription and transcript stability (*5*, *6*). Numerous similarities, including the involvement of noncoding RNAs, can be found between XCI and RNAi silencing of constitutive heterochromatin. However, a deficiency of Dicer (Dcr) has no obvious effect on maintaining Xi in T cells (*7*) and, although Xist and Tsix RNAs are perfectly complementary, dsRNAs had never been observed in vivo.

Here, we formally explore a role for RNAi in XCI. To search for small RNAs (sRNAs) within *Xist/Tsix*, we performed Northern analysis in mouse embryonic stem (ES) cells, a model that recapitulates XCI during cell differentiation ex vivo; and in mouse embryonic fibroblasts (MEFs), post-XCI cells that faithfully maintain one Xi. At repeat A, a region of *Xist* required for silencing (*8*), we observed sRNAs at ~30 nucleotides (nt) and ~37 nt in the Tsix orientation and at ~25 and ~35 nt in the Xist orientation (Fig. 1A). At *Xist* exon 7, sRNAs occurred between 24 and 42 nt on the Tsix strand and at ~25 and ~35 nt on the Xist strand (Fig. 1B). At the promoter, robust quantities of Tsix-strand sRNAs were observed (Fig. 1C). sRNAs were also seen on the Xist strand, implying that low-level sense transcription must occur at the promoter. The integrity of all Northern blots was confirmed by micro RNA 292-as (miRNA292-as) and tRNA controls (Fig. 1 and fig. S1). The sRNAs were developmentally regulated, being unmeasurable in the pre-XCI [day 0 (d0)] and post-XCI (MEF) states and detectable only during XCI (d4 and d10). Furthermore, sRNAs occurred in both XX and XY cells. For discussion purposes, we call them xiRNA for their X-inactivation center origin, distinct from the smaller small interfering RNA (siRNAs) and miRNAs.

To determine whether xiRNA production depends on antisense expression, we investigated ES cells in which *Tsix* was deleted ($Tsix^{\Delta CpG}$) (*4*) and the *Tsix* regulator *Xite* ($Xite^{\Delta L}$) (*9*). Deleting *Tsix* resulted in a dramatic reduction in antisense-strand xiRNA (Fig. 1D). A residual level of xiRNA was still detectable, consistent with cryptic promoter activity in $Tsix^{\Delta CpG}$ (*4*). Deleting *Xite* likewise reduced antisense xiRNA levels, consistent with a requirement for *Xite* in transactivating *Tsix* (*9*). In the sense orientation, both deletions also compromised xiRNA production. Thus, sRNAs are indeed generated from *Xist/Tsix* and depend on *Tsix* and *Xite* expression.

The presence of xiRNAs implied that Tsix and Xist must exist as long duplex precursors. However, the developmental timing of xiRNA appearance is paradoxical: Although Tsix and Xist are biallelically expressed on d0, they become monoallelically expressed on opposite Xs during XCI (*4*). On d0, three to five copies per chromosome of Xist RNA are present, whereas Tsix occurs at >10-fold molar excess (*10*–*12*). Upon XCI, Tsix is down-regulated on Xi as Xist up-regulates >30-fold. On Xa, Tsix persists as Xist is down-regulated. How would dsRNA form when Tsix and Xist, both cis-limited, are on opposite chromosomes during XCI?

Department of Molecular Biology, Massachusetts General Hospital; Department of Genetics, Harvard Medical School; and Howard Hughes Medical Institute, Boston, MA 02114, USA.

*To whom correspondence should be addressed. E-mail: lee@molbio.mgh.harvard.edu

To determine whether Tsix and Xist formed dsRNA, we devised an in vivo ribonuclease (RNase) protection assay based on differential susceptibility of single-stranded RNA (ssRNA) and dsRNAs to RNase A/T1. We permeabilized replicate preparations of d0 ES cells in a non-denaturing buffer containing deoxyribonuclease I (DNase I) and RNase, and performed strand-specific reverse transcription polymerase chain reaction (RT-PCR) on the protected RNAs. To confirm assay sensitivity, a positive control into which one copy per cell of in vitro–transcribed

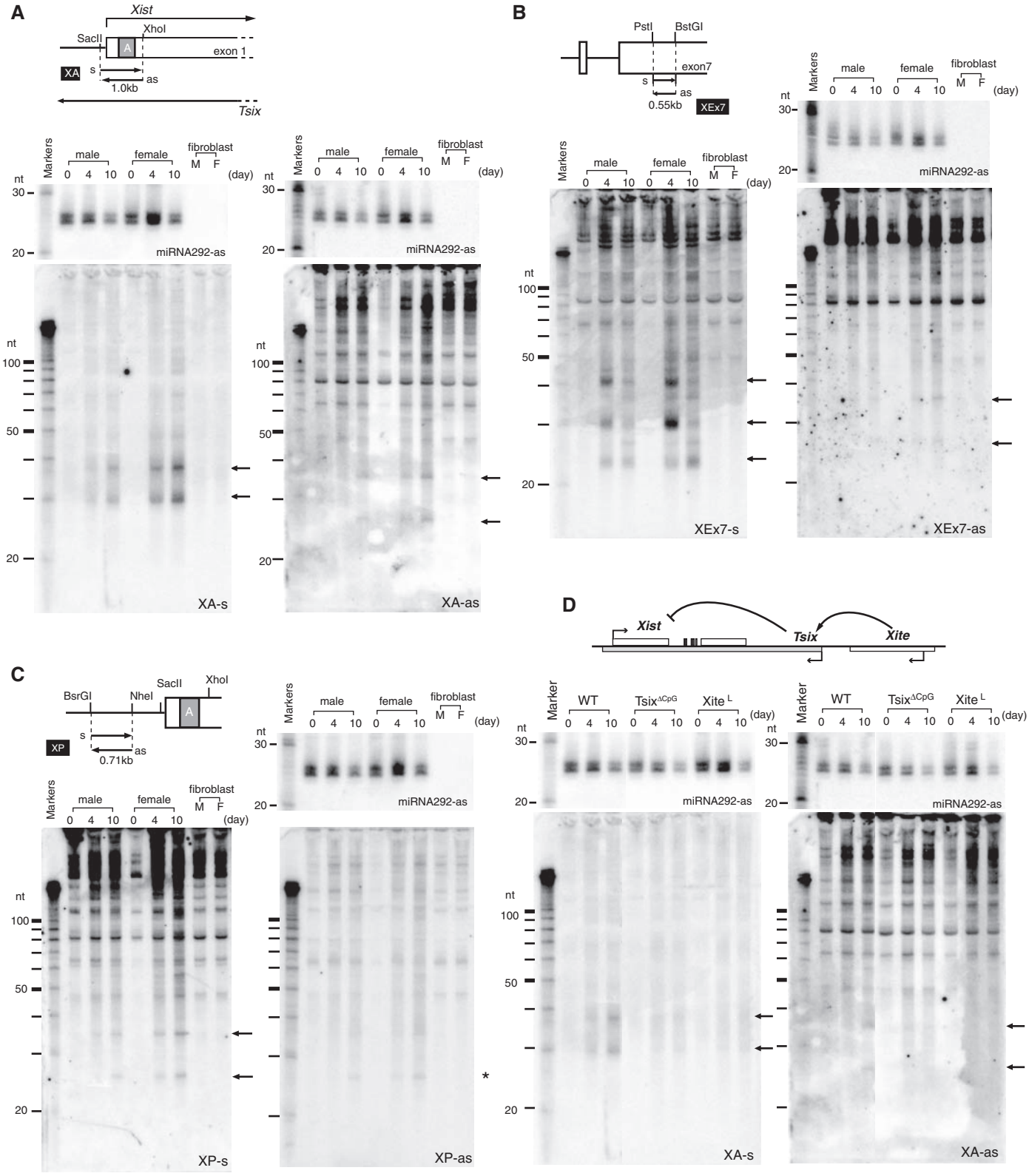

Fig. 1. sRNAs derived from *Tsix/Xist*. (**A**) xiRNAs from *Xist* repeat A (XA) region (map) detected by Northern analysis. Sense (s) and antisense (as) riboprobes detected Tsix and Xist, respectively. miR292-as controls are shown on the same blots. M, male; F, female. (**B**) Northern analysis of xiRNAs from *Xist* exon 7 (XEx7). (**C**) Northern analysis of *Xist* promoter (XP) region. (**D**) Northern analysis of mutant cells. WT lanes are identical to those in (A) (concurrent analysis).

and annealed Tsix:Xist dsRNA was spiked could readily be detected with this protocol (Fig. 2, A and B). The abundant single-stranded ribonucleotide reductase M2 (Rrm2) and glyceraldehyde-3-phosphate dehydrogenase (Gapdh) transcripts were not amplified, indicating that our assay was specific for dsRNA. We consistently observed RNase-protected Xist and Tsix RNA strands in XX and XY ES cells, suggesting the presence of dsRNA (Fig. 2B). Real-time RT-PCR quantitation showed that ~16% of Xist and ~13% of Tsix strands were protected (Fig. 2C). As expected of duplexes, approximately equal stoichiometric ratios of the two strands were present in the RNase-protected fraction. Kinetic analysis revealed decreasing amounts of dsRNA during differentiation in XX and XY cells (Fig. 2D). Thus, steady-state quantities of both dsRNA and xiRNA are developmentally regulated, but in an opposite manner.

The inverse correlation over time raised the possibility that dsRNA is processed to xiRNA. To address potential allelic differences, we performed allele-specific RNase protection assays using two genetically marked female ES cell lines: wild-type (WT) 16.7, which carries Xs from *Mus castaneus* (X^{cas}) and *M. musculus* (X^{mus}) and undergoes random XCI [with a natural 30:70 specific-specific bias (*13*)], and $Tsix^{\Delta CpG/+}$ mutants, which harbor a *Tsix* deletion on X^{mus} (*4*) and therefore always inactivate X^{mus} in the 16.7 background. Total Tsix RNA (with no RNase treatment) decreased >10-fold over time, but a low residual level could still be detected at d4 and d10 as expected (*4*, *9*, *14*). From this residual pool, using single-nucleotide polymorphism (SNP)–based allele-specific primers at position 3, we unexpectedly found that duplexed Tsix (RNase-protected) in $Tsix^{\Delta CpG/+}$ cells predominantly originated from Xi (X^{mus}) (Fig. 2E), the X on which the major *Tsix* promoter is deleted. Likewise, the Xist strand found in duplex form originated from Xi. Thus, Tsix:Xist duplexes are detected primarily from Xi.

Duplexes may form only on Xi, or they may form on both Xs but be stable only on Xi. The latter possibility is notable, considering the inverse kinetic relationship between the appearance of long dsRNA versus xiRNA. Could dsRNA be processed to xiRNA on Xa? Several observations favored this idea. First, dsRNA was selectively lost from Xa. Second, xiRNA production depended on *Tsix*, a gene expressed from Xa from d4 to d10. Finally, despite lacking Xi, XY cells produced xiRNAs.

Because dsRNAs are substrates for Dcr, we tested Dcr's role by deleting *Dcr*'s RNAseIII domain in female ES cells (*15*) (fig. S2). Because Dcr-deficient ($Dcr^{-/-}$) cells are known to grow poorly (*15*), we introduced a *Dcr* transgene expressed at <<5% of WT levels (Fig. 3, A and B) and improved the growth of $Dcr^{-/-}$ clones (henceforth referred to as $Dcr^{-/-}$). Northern analysis revealed diminished xiRNA levels (Fig. 3, C and D), suggesting that xiRNA production depends on Dcr. All tested *Dcr*-deficient clones behaved similarly. *Xist* expression prematurely increased 5- to 10-fold in pre-XCI cells (Fig. 3B), implying increased *Xist* transcription or greater RNA stability. Male $Dcr^{-/-}$ clones likewise showed significant Xist derepression on d4 (fig. S3). Thus, Dcr regulates xiRNA levels and antagonizes *Xist* upregulation in ES cells.

RNA immunofluorescence in situ hybridization (immunoFISH) analysis showed that Dcr has

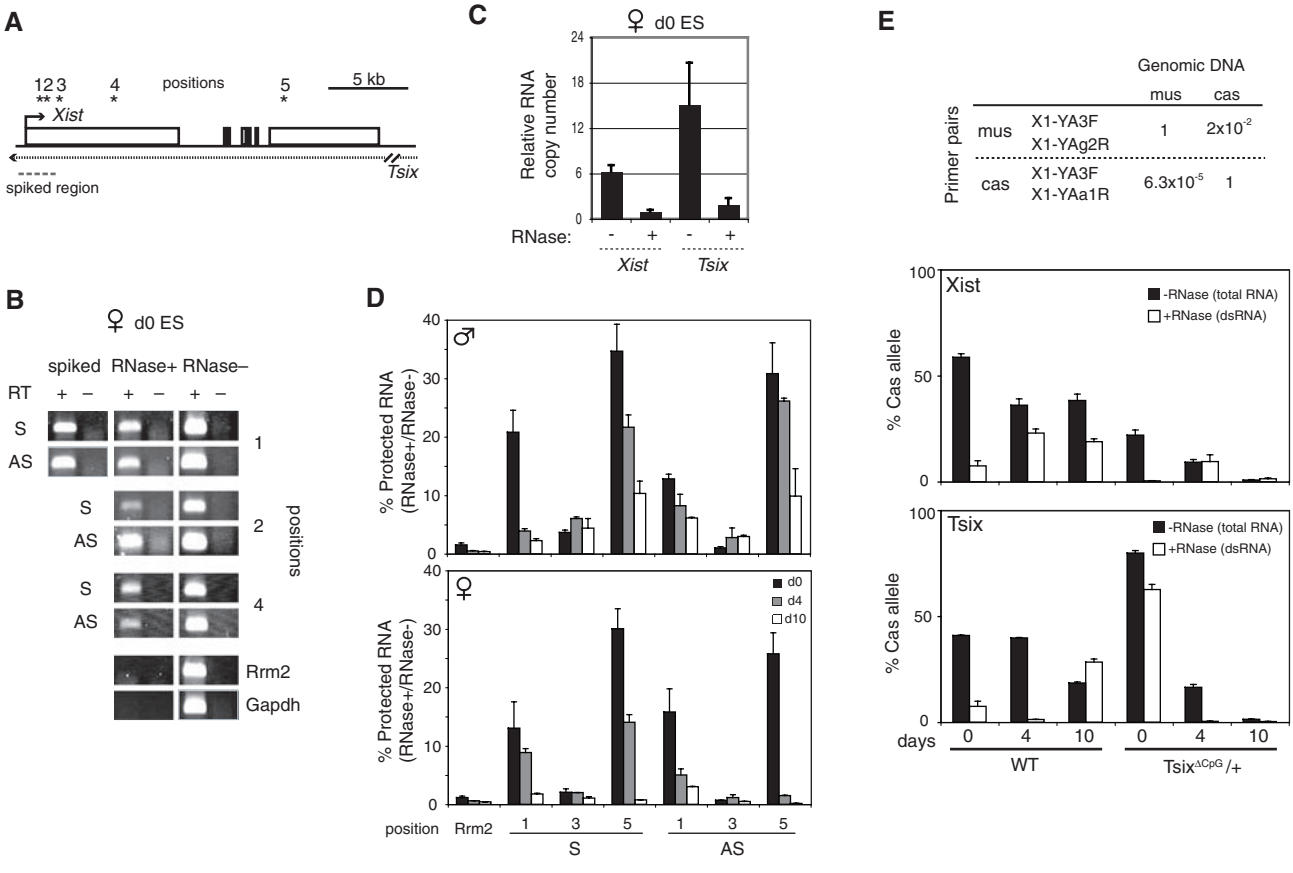

Fig. 2. Tsix and Xist RNA form long duplexes in vivo. (**A**) Map of *Tsix/Xist* and primer pairs (asterisks). (**B**) In vivo RNAse protection assay. (**C**) Relative quantities of Xist and Tsix in duplexes measured at position 2 (base pairs 1206 to 1337 of *Xist*) by strand-specific real-time RT-PCR of protected RNA ($RNase^+$) as compared with total levels ($RNase^-$). Quantities are standardized to Xist in the Xist-Tsix duplex (for Xist, $RNase^+ = 1$). Error bars indicate 1 SD in triplicate reactions. (**D**) Quantities of protected Tsix or Xist RNAs ($RNase^+$) relative to total Tsix or Xist ($RNase^-$) for in vivo RNase protection assays. Error bars indicate 1 SD in triplicate reactions. (**E**) In vivo RNase protection assays to test allelic origin of dsRNA using strand-specific, allele-specific real-time RT-PCR with SNP-based primers for X^{cas} or X^{mus} alleles (top). PCR of control genomic DNA shows high specificity (98% for mus and >99.99% for cas). Error bars indicate 1 SD in triplicate reactions. For test samples, the mus and cas fractions were amplified separately, normalized to genomic DNA (X^{cas}:X^{mus} = 1:1), and plotted as a function of time. Percent of Cas = [X^{cas} RNA/(X^{cas} RNA + X^{mus} RNA)] × 100. Because the bars show relative allelic fractions, quantities are only comparable within a single time point.

additional XCI effects. Despite elevated Xist levels, Xist could not "coat" the X nor induce heterochromatic changes (Fig. 3E). On d10, Xist RNA accumulation occurred in only 0.4% of cells (n = 278 cells) and histone 3 (H3) lysine 27 (K27) trimethylation (H3-3meK27) in 0.7% of cells (n = 278 cells). By contrast, in *Dcr* 2lox/– [heterozygous Dcr knockout carrying one conditional allele (2loxP sites) and one deleted allele] controls, Xist accumulated in 56.8% and H3-3meK27 in 83.1% of cells (n = 148 cells). Moreover, the X-linked *Mecp2* gene failed to be dosage-compensated in $Dcr^{-/-}$ cells, whereas it appropriately decreased 1.5- to twofold in controls (Fig. 3A). Therefore, in addition to local effects on *Xist*, Dcr also affected Xi globally, because the formation of Xist and H3-3meK27 domains was compromised without Dcr.

Because XCI and cell differentiation are linked (*16*, *17*), the XCI defects might be explained by Dcr's pleiotropic effects on differentiation (*15*, *18*) rather than specific effects on XCI. Indeed, $Dcr^{-/-}$ clones differentiated poorly and continued to express Oct4 and Nanog pluripotency factors on d10 (Fig. 3, A and F, fig. S3). To determine whether Dcr specifically affects XCI, we truncated Tsix by inserting a polyadenylate cassette in $Dcr^{-/-}$ cells (fig. S4), reasoning that disabling *Tsix*, which negatively regulates *Xist*, might overcome the failure to accumulate Xist RNA. As expected, $Dcr^{-/-}Tsix^{-/+}$ double mutants (Dcr-TST) and $Tsix^{-/+}$ controls (TST) showed truncated Tsix expression from X^{mus} and highly skewed XCI patterns (Fig. 4A). Although Dcr-TST cells continued to differentiate poorly (fig. S5), total Xist levels were restored to nearly WT levels during differentiation (Fig. 4B). Furthermore, disabling Tsix partially restored Xist localization to Xi (Fig. 4C). Therefore, Dcr's effect on XCI can be genetically separated from its effect on cell differentiation.

Additionally, to the extent that Xist levels and localization were restored in Dcr-TST cells, H3-3meK27 was only partly rescued in $Xist^{+}$ cells (Fig. 4D). In WT and TST controls, Xist accumulation was almost always accompanied by robust H3-3meK27. In contrast, 30 to 40% of $Xist^{+}$ Dcr-TST cells displayed weak or no H3-3meK27 foci, implying that H3-3meK27 also depends on Dcr. These data showed that Xist accumulation and H3-K27 methylation are genetically separable. We conclude that Dcr intersects XCI in several ways. Locally, Dcr controls xiRNA and Xist expression. Globally, it regulates Xist accumulation and H3-3meK27 on Xi.

In aggregate, our data suggest specific effects of RNAi on XCI (Fig. 4E). *Dcr* and *Tsix/Xist* genetically interact, and a second-site mutation in *Tsix* partially suppresses the $Dcr^{-/-}$ effect on *Xist.* We propose that Tsix:Xist duplexes initially form on both Xs. During XCI, continued expression of Tsix on Xa would lead to dsRNA processing to xiRNAs, which would locally repress *Xist* in cis, an idea reminiscent of transcriptional gene silencing (TGS) (*6*, *19*–*21*). Consistent with allele-specific TGS at *Xist*, RNA-directed DNA methyl-

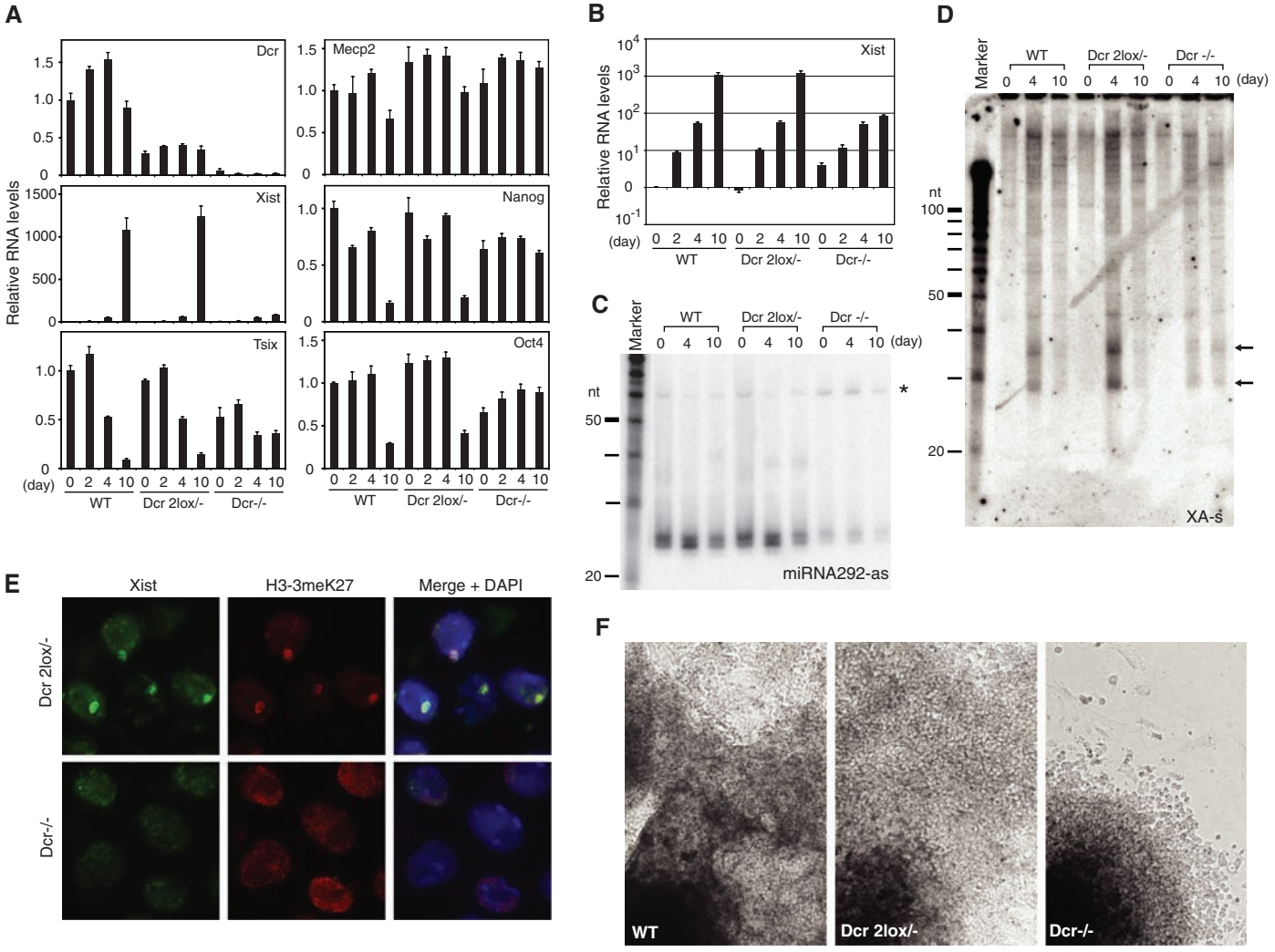

Fig. 3. *Dcr* deficiency impairs xiRNA production and XCI. (**A**) Quantitative real-time RT-PCR of indicated transcripts normalized to β-actin. (**B**) Xist quantitation plotted on a log scale. (**C** and **D**) Northern analyses of miRNA292-as control (C) and xiRNAs (D) in mutant cells. There is an accumulation of miRNA292-as precursors (asterisk) in $Dcr^{-/-}$ cells. (**E**) Immuno-RNA FISH for Xist and H3-3meK27 on d10. 4′,6′-diamidino-2-phenylindole (DAPI), blue. (**F**) Phase contrast images of d10 embryoid bodies (EB).

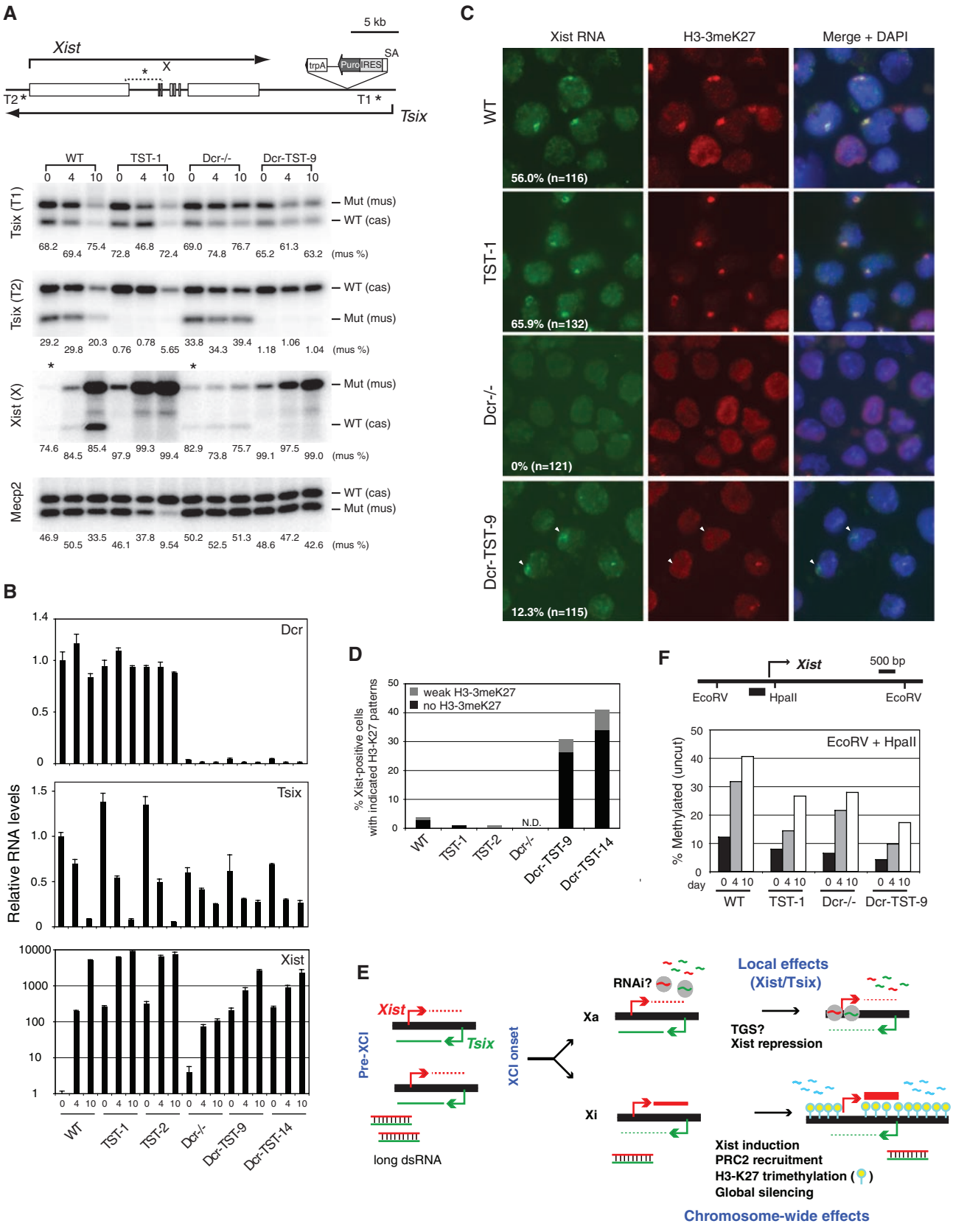

Fig. 4. *Tsix* genetically interacts with *Dcr*. (**A**) Allele-specific RT-PCR analysis. All RT reactions were negative (not shown in figure). Xist d0 samples (asterisks) were 10-fold overloaded to visualize low expression. trpA, triple poly-A cassette; Puro, puromycin; IRES, internal ribosome site; SA, splice acceptor. (**B**) Real-time RT-PCR of indicated transcripts, each normalized to β-actin. (**C**) Immuno-RNA FISH for Xist and H3-3meK27 domains (arrowheads) on d10. *n*, sample size. (**D**) Frequency of aberrant H3-3meK27 enrichment in the Xist$^+$ subpopulation of indicated cell lines. $n = 100$ to 150 cells. (**E**) Model of the intersection of RNAi and XCI. (**F**) Methylation-sensitive restriction analysis of the *Xist* promoter. Genomic DNA was digested with EcoRV or Eco RV+Hpa II. The percent of uncut (methylated) DNA at Hpa II is plotted.

ation by *Tsix* has been proposed (*10*). Here we found that abrogating Dcr and/or Tsix resulted in decreased methylation at the 5′ end of *Xist* (Fig. 4F). By our model, extremely low Tsix and Xist expression might be sufficient to maintain TGS on Xa in post-XCI cells (*19*). On Xi, chromosome-wide accumulation of Xist RNA and H3-3meK27 depends on Dcr. These ideas support the emerging concept of nuclear RNAi processes in mammals (*20*, *21*). Because Dcr is not known to cleave RNAs to 25 to 42 nt, the observed effects on XCI may be partially indirect. Alternatively, Dcr may have properties yet to be discovered in mammals. XCI now provides a new system in which to investigate RNAi processes.

References and Notes

1. M. F. Lyon, *Nature* **190**, 372 (1961).
2. C. J. Brown *et al.*, *Cell* **71**, 527 (1992).
3. G. D. Penny, G. F. Kay, S. A. Sheardown, S. Rastan, N. Brockdorff, *Nature* **379**, 131 (1996).
4. J. T. Lee, N. Lu, *Cell* **99**, 47 (1999).
5. A. Fire *et al.*, *Nature* **391**, 806 (1998).
6. S. I. Grewal, S. C. Elgin, *Nature* **447**, 399 (2007).
7. B. S. Cobb *et al.*, *J. Exp. Med.* **201**, 1367 (2005).
8. A. Wutz, T. P. Rasmussen, R. Jaenisch, *Nat. Genet.* **30**, 167 (2002).
9. Y. Ogawa, J. T. Lee, *Mol. Cell* **11**, 731 (2003).
10. B. K. Sun, A. M. Deaton, J. T. Lee, *Mol. Cell* **21**, 617 (2006).
11. C. H. Buzin, J. R. Mann, J. Singer-Sam, *Development* **120**, 3529 (1994).
12. S. Shibata, J. T. Lee, *Hum. Mol. Genet.* **12**, 125 (2003).
13. P. Avner *et al.*, *Genet. Res.* **72**, 217 (1998).
14. S. Shibata, J. T. Lee, *Curr. Biol.* **14**, 1747 (2004).
15. E. P. Murchison, J. F. Partridge, O. H. Tam, S. Cheloufi, G. J. Hannon, *Proc. Natl. Acad. Sci. U.S.A.* **102**, 12135 (2005).
16. M. Monk, M. I. Harper, *Nature* **281**, 311 (1979).
17. J. T. Lee, *Science* **309**, 768 (2005).
18. C. Kanellopoulou *et al.*, *Genes Dev.* **19**, 489 (2005).
19. T. A. Volpe *et al.*, *Science* **297**, 1833 (2002).
20. D. H. Kim, L. M. Villeneuve, K. V. Morris, J. J. Rossi, *Nat. Struct. Mol. Biol.* **13**, 793 (2006).
21. K. V. Morris, S. W. Chan, S. E. Jacobsen, D. J. Looney, *Science* **305**, 1289 (2004).

22. We thank G. Hannon for the *Dcr* targeting construct and Dcr2lox/$^{-}$ male ES cells; N. Lau for technical advice; and M. Anguera, J. Erwin, S. Namekawa, B. Payer, and J. Zhao for careful critique of the manuscript. Y.O. is especially indebted to A. Ogawa for her support. This work is funded by the Medical Scientist Training Program (B.K.S.), NIH, and the Howard Hughes Medical Institute (J.T.L.).

Supporting Online Material

www.sciencemag.org/cgi/content/full/320/5881/1336/DC1
Materials and Methods
Figs. S1 to S5
References

12 March 2008; accepted 30 April 2008
10.1126/science.1157676

Fission Yeast Pot1-Tpp1 Protects Telomeres and Regulates Telomere Length

Tomoichiro Miyoshi, Junko Kanoh, Motoki Saito, Fuyuki Ishikawa*

Telomeres are specialized chromatin structures that protect chromosomal ends. Protection of telomeres 1 (Pot1) binds to the telomeric G-rich overhang, thereby protecting telomeres and regulating telomerase. Mammalian POT1 and TPP1 interact and constitute part of the six-protein shelterin complex. Here we report that Tpz1, the TPP1 homolog in fission yeast, forms a complex with Pot1. Tpz1 binds to Ccq1 and the previously undiscovered protein Poz1 (Pot1-associated in *Schizosaccharomyces pombe*), which protect telomeres redundantly and regulate telomerase in positive and negative manners, respectively. Thus, the Pot1-Tpz1 complex accomplishes its functions by recruiting effector molecules Ccq1 and Poz1. Moreover, Poz1 bridges Pot1-Tpz1 and Taz1-Rap1, thereby connecting the single-stranded and double-stranded telomeric DNA regions. Such molecular architectures are similar to those of mammalian shelterin, indicating that the overall DNA-protein architecture is conserved across evolution.

Telomeres consist of long arrays of double-stranded (ds) G-rich telomeric repeats terminated by G-rich single-stranded (ss) overhangs at the 3′-terminus (G-tail). The *Oxytricha nova* telomere end–binding protein (TEBP)–α and –β heterodimers are prototypes of G-tail–binding proteins (*1*, *2*). TEBP-α and -β contain oligonucleotide/oligosaccharide-binding (OB) fold domains involved in DNA binding and protein-protein interaction (*3*). Protection of telomeres 1 (Pot1), the homolog of TEBP-α, binds to the G-tail and is essential for telomere protection (*4*, *5*). Mammalian POT1 and the TEBP-β homolog TPP1 form a complex that protects telomeres and regulates telomerase (*6*–*9*). POT1 and TPP1 constitute the shelterin complex together with TIN2, RAP1, and ds telomeric DNA–binding proteins TRF1 and TRF2 (*10*). It has been proposed that mammalian POT1 transduces signals from TRF1 to negatively control telomerase reaction (*11*).

To elucidate how fission yeast Pot1 functions, we purified proteins associated with Pot1. We identified Ccq1 and two uncharacterized proteins, encoded SPAC19G12.13 and SPAC6F6.16, by mass spectrometry of Pot1 immunoprecipitates (fig. S1 and table S1). Ccq1 is a telomere protein that recruits a Snf2/histone deacetylase (HDAC)–containing repressor complex (SHREC) (*12*, *13*). SPAC19G12.13 produces the previously undiscovered Pot1 complex component Poz1 (Pot1-associated in *Schizosaccharomyces pombe*) (GenBank accession number AB433171). We found that the presence of introns in SPAC6F6.16 resulted in encoding a protein larger than that predicted in the database (fig. S2). Secondary structure–based fold-recognition programs predicted that the N terminus of the SPAC6F6.16 product (residues 1 to 158) contains an OB fold domain that is most closely related to those of TEBP-β and human TPP1 (fig. S2 and table S3). Moreover, the product and Pot1 form a complex that protects telomeres and regulates telomerase. We therefore conclude that SPAC6F6.16 encodes the fission yeast Tpp1 homolog. Because the gene name *tpp1*$^{+}$ is already being used by another gene in fission yeast, we will call this gene *tpz1*$^{+}$ (*TPP1 homolog* in Schizosaccharomyces pombe) (GenBank accession number AB433170).

The physical association between Pot1 and Ccq1, Tpz1, or Poz1 was confirmed by immunoprecipitation (Fig. 1A). Immunofluorescence experiments showed that Ccq1, Tpz1, and Poz1 colocalize with Pot1 (fig. S3). A chromatin immunoprecipitation (ChIP) assay also demonstrated that Ccq1, Tpz1, and Poz1 are specifically bound to telomeres (Fig. 1B). Thus, Ccq1, Tpz1, and Poz1 are closely associated with Pot1 at telomeres. Ccq1 directly associates with Clr3, an HDAC in SHREC (*12*) (fig. S4). However, Clr3 was not detected in the Pot1-precipitated fraction and is not involved in controlling telomere length, indicating that the Pot1 complex identified in this study is distinct from SHREC.

We used a yeast two-hybrid assay to examine interactions between Tpz1 and Pot1, Ccq1, or Poz1. Tpz1 associated with Pot1, Ccq1, and Poz1 (Fig. 1C). However, we did not observe any substantial interaction between Poz1 and Pot1 or Ccq1 (fig. S5). Deletion analyses revealed that the N terminus of Tpz1 (amino acids 2 to 223) is sufficient for the interaction with Pot1 but not with Ccq1 or Poz1 [Pot1-binding domain (PBD)]. The N-terminal OB fold (OB1) of Pot1 (amino acids 1 to 138) is dispensable for the interaction. In contrast, the C terminus of Tpz1 (amino acids 379- to 508) interacts with Ccq1 and Poz1 but not with Pot1[Ccq1/Poz1-binding domain (CPBD)]. Taken together, Tpz1 is the core molecule interacting with Pot1, Ccq1, and Poz1. The relative positions of the regions responsible for Pot1-Tpz1 interaction in Pot1 and Tpz1 are similar to those in TEBP-α/β and human TPP1 and POT1

Department of Gene Mechanisms, Graduate School of Biostudies, Kyoto University, Yoshida-Konoe-cho, Sakyo-ku, Kyoto 606-8501, Japan.

*To whom correspondence should be addressed. E-mail: fishikaw@lif.kyoto-u.ac.jp

Intersection of the RNA Interference and X-Inactivation Pathways

Yuya Ogawa, Bryan K. Sun and Jeannie T. Lee

Science **320** (5881), 1336-1341.
DOI: 10.1126/science.1157676